Journal of Applied Electrochemistry (2024) 54:1845–1859
https://doi.org/10.1007/s10800-024-02072-5

RESEARCH ARTICLE

Designing and characterization of a novel sensing platform based on Zn-doped Fe_3O_4 nanosheets/graphene oxide nanocomposite for enhanced electrochemical determination of guanine and adenine simultaneously

Rahem Nouraei[1] · **Ali Babaei**[1,2]

Received: 20 September 2023 / Accepted: 13 January 2024 / Published online: 28 February 2024

Abstract

In this study, a new electrochemical sensor using a glassy carbon electrode modified with graphene oxide (GO) and Zn-doped magnetite Fe_3O_4 nanosheets is proposed for simultaneous trace determinations of guanine (GA) and adenine (AD). First, graphene oxide nanoparticles were synthesized by the Hammer method, and then UV–Vis, FTIR, and XRD techniques were used to characterize them. The second step involved hydrothermal preparation of Zn-doped magnetite Fe_3O_4 nanosheets. Different methods, such as scanning electron microscopy, transmission electron microscopy, Fourier transform infrared spectroscopy (FTIR), vibrating sample magnetometer, and energy dispersive X-ray spectroscopy, were utilized to investigate Zn-doped magnetite Fe_3O_4 nanosheets. The electrochemical behavior of guanine (GA) and adenine (AD) was investigated using different voltammetric techniques, including cyclic voltammetry, electrochemical impedance spectroscopy, differential pulse voltammetry, and chronoamperometry (CA). It was found that by combining GO with Zn-doped magnetite Fe_3O_4 nanosheets, the electrochemical sensitivity of the sensor can be improved, and low levels of guanine and adenine can be measured. In a differential pulse voltammetry experiment conducted with this electrode under optimal conditions, such as buffer type, accumulation time, and PH, the electrode showed great sensitivity to both guanine and adenine. The detection limit values were 0.08 and 0.14 µM for GA and AD, respectively. The suggested sensor's performance was tested using human serum as a real sample, and the proposed sensor showed high recovery. As a result of the investigation, it was found that the proposed electrode displayed high sensitivity, good repeatability, and high stability.

Graphical abstract

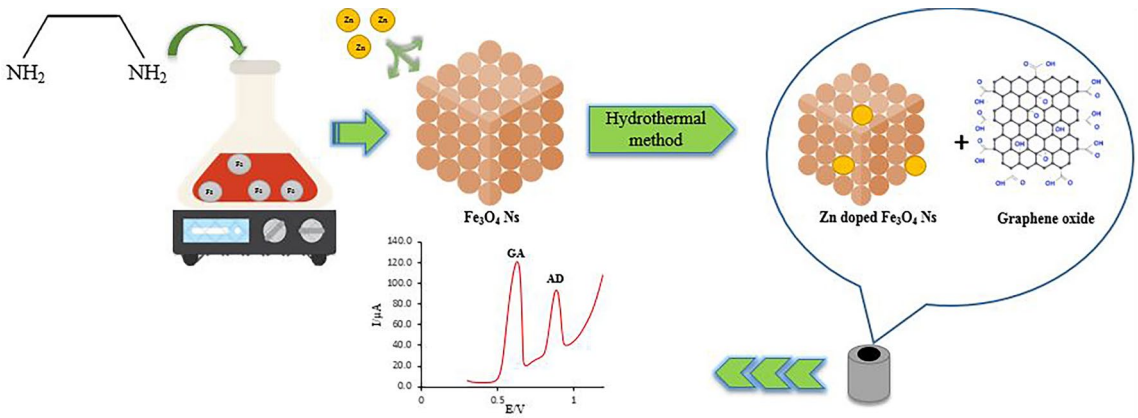

Keywords Electrochemical sensor · Graphene oxide (GO) · Zn-doped magnetite Fe_3O_4 nanosheets · Guanine · Adenine

Extended author information available on the last page of the article

1 Introduction

An increasing number of electrochemical sensors are made of graphene oxide (GO), a two-dimensional carbon lattice with functional groups such as hydroxyl and carbonyl groups. As a result of its large surface area, chemical stability, electrical conductivity, and other advantages, graphene is one of the most advantageous nanomaterials for simplifying and modifying electrodes [1]. So, it can be demonstrated that nanomaterials like graphene oxide can significantly improve the sensitivity of electrochemical sensors by providing stable and well-organized platforms [2–4]. Graphene-based sensors are promising for biomolecule detection due to their unique properties. They have been used to detect DNA, proteins, enzymes, and metabolites with high sensitivity. Functionalization with specific recognition elements and the use of composite materials have further enhanced their capabilities. Overall, graphene-based sensors are valuable for biomedical research, clinical diagnostics, and environmental monitoring [5–8].

ZnO, a wide-band gap semiconductor, has attracted attention due to its high surface area, biocompatibility, and low toxicity. ZnO-based electrochemical sensors have been used for the detection of various analytes, such as heavy metals, pesticides, and neurotransmitters, with high sensitivity and selectivity [9–11]. Iron oxide nanostructures have also attracted increasing interest because of their high catalytic activity and low toxicity, making them an appealing material for constructing chemical and biological sensors. Various techniques can be employed to create different iron oxide nanostructure shapes, including sol–gel [12], hydrothermal/solvothermal [13], electrospray [14], microemulsions [15], and flow injection [16]. It is possible to functionalize, composite, or dope magnetic iron nanostructures with other metals to enhance their stability and electrochemical activity. Doping Fe_3O_4 to modify the electrochemical sensor can increase its sensitivity by amplifying the signal response [17]. The presence of Fe_3O_4 can enhance electron-transfer kinetics, resulting in a more efficient detection process and improved sensor performance [18]. In general, dopants can act as a stabilizer and enhance stability and durability, reducing the degradation of the sensor over time [19]. This can result in a longer lifespan and more reliable measurements. Zn^{2+} metal ions are one of the most efficient metal doping ions in iron oxide nanostructures because they do not damage the crystal structure. In recent years, composite formation between metal-doped iron nanostructures and graphene oxide has become a hot research topic because of the new and enhanced functionalities of iron nanostructures and graphene.

The biosynthesis of proteins and the storage of genetic information rely on deoxyribonucleic acid (DNA). Life processes rely on nucleotides as energy carriers, messengers, and assistants to activate enzymes. Deoxyribonucleic acid contains important components (bases or nucleotides), guanine (Fig. S1), and adenine (Fig. S2). There may be various diseases present in the body because of unusual alterations in the organism's bases, which point to a defect or mutation in the immune system. Thus, bioscience and clinical diagnosis-depend significantly on analyzing these bases. To detect and quantify purine bases in nucleic acids, numerous techniques have been created. These include high-performance liquid chromatography (HPLC) [20], capillary electrophoresis (CE) [21], spectroscopic methods [22, 23], chemiluminescence (CL) [24], and mass spectrometry (MS) [25]. However, the electrochemical technique is attractive due to its high sensitivity, ease of preparation, and rapid and low cost compared to the other methods for determining guanine and adenine. The determination of guanine and adenine, however, must be improved through the development of new and efficient methods that are convenient.

In this work for the first time a new sensor based on Zn-doped Fe_3O_4 nanosheets and graphene oxide modified glassy carbon (Zn-doped Fe_3O_4/GO/GCE) was used for the electrochemical determination of guanine (GA) and adenine (AD). The use of magnetic Fe_3O_4 nanosheets in electrochemical sensor development is a major breakthrough in materials science and analytical chemistry. The electrochemical behavior of GA and AD was investigated using different voltammetric techniques, including cyclic voltammetry (CV), electrochemical impedance spectroscopy (EIS), differential pulse voltammetry (DPV), and chronoamperometry (CA). The method employed in this research reduces the need for complex equipment and time for synthesis while exhibiting superior properties compared to conventional nanoparticles. It appears that combinations of Zn-doped Fe_3O_4 nanosheets and graphene oxide improve the electrode's sensitivity for detecting GA and AD, offering promising prospects for the future of electrochemical analyses. Additionally, Zn ions can enhance the electrochemical performance and the structural stability of Fe_3O_4 nanosheets. According to the investigation results, the modified electrode possessed high sensitivity, repeatability, and stability for determining GA and AD.

2 Experimental

2.1 Chemicals

In this research, Zn-doped Fe_3O_4 nanosheets were synthesized using analytical grades, including zinc nitrate

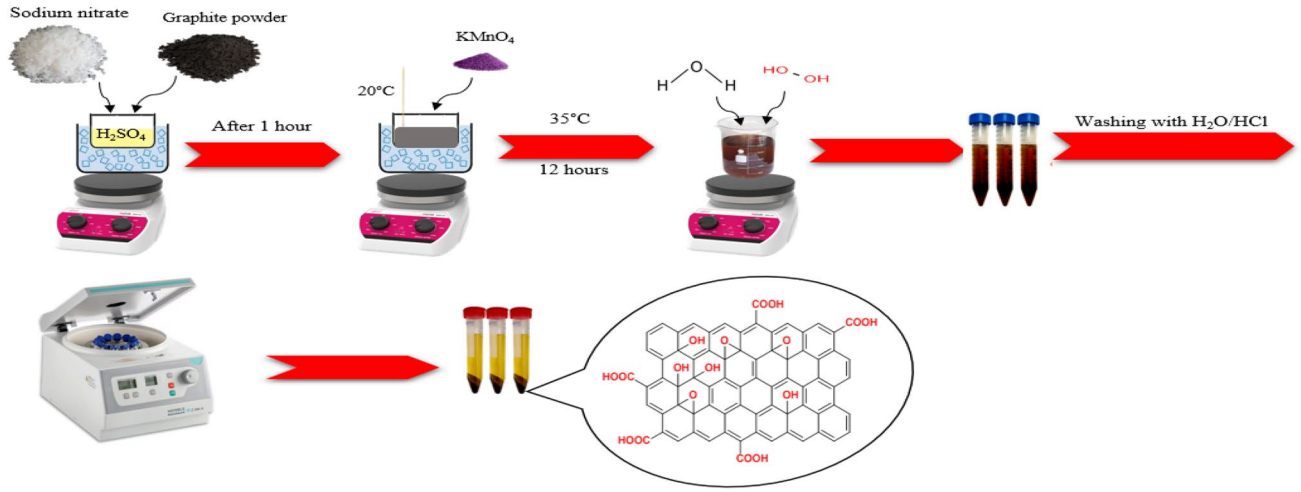

Scheme 1 The schematic procedures for the synthesis of graphene oxide (GO)

hexahydrate ($Zn(NO_3)_2{\cdot}6H_2O$), ethylenediamine ($C_2H_8N_2$), ethylene glycol ($C_2H_6O_2$), sodium acetate (CH_3COONa), and ferric nitrate nonahydrate ($Fe(NO_3)_3{\cdot}_9H_2O$) supplied by Merck. The ingredients used to synthesize graphene oxide, including pure graphite powder, sodium nitrate ($NaNO_3$), concentrated sulfuric acid (H_2SO_4), potassium permanganate ($KMnO_4$), and hydrogen peroxide 30% (H_2O_2 30%), were purchased from Merck. Alumina powder from Merck Company was used to clean the electrode surface. Guanine (GA) and adenine (AD) are provided by Sigma-Aldrich Co. To prepare Britton–Robinson buffers, we used the following materials: NaOH, acetic acid (99.5%), H_3PO_4 (75%), and H_3BO_3 (99.8% ACS reagent, Sigma-Aldrich). All of the solutions were made with double-distilled water.

2.2 Instrumentation

Several electrochemical experiments were conducted using an electrode array consisting of three electrodes: a working electrode (GO/Zn-doped magnetite Fe_3O_4Ns/GCE), an auxiliary electrode (platinum wire), and a reference electrode (Ag/AgCl). Electrochemical tests were carried out using a Potentiostat/Galvanostat Autolab PGSTAT 30 (EcoChemie, The Netherlands). A PW173 X-ray diffraction instrument was used for analyzing the XRD patterns. For the visualization of nanosheets, TEM images were taken with an acceleration voltage of 100 kV on an EM10C device from Zeiss Germany. The Zeiss Germany model Sigma VP was used to perform FESEM, EDS, and mapping analysis to analyze morphological patterns and elements. Perkin Elmer's 543 FTIR spectrometer was used to record the spectra.

2.3 Graphene oxide synthesis

Graphene oxide (GO) was synthesized utilizing a modified Hummer's technique with graphite powder as a starting material. A flask in the ice bath was filled with 23 ml of concentrated sulfuric acid. 1 g of graphite and 0.5 g of sodium nitrate were added to the solution, and the mixture was vigorously stirred (Scheme 1). After 1 h, using an ice bath to maintain the temperature below 20 °C, 3 g of $KMnO_4$ were slowly added to the above solution to avoid overheating and explosion. After 12 h of stirring at 35 °C, the mixture became brown. The solution was diluted and treated with 5 ml of a 30% H_2O_2 solution after 500 ml of water had been added while being vigorously stirred. Graphene oxide sheets were obtained after centrifugation and washing several times with H_2O and diluted HCl, followed by filtration and drying [26].

2.4 Synthesis of Zn-doped Fe_3O_4 magnetic nanosheets

The first step was to add 25 ml of anhydrous ethylene glycol to a 50 ml beaker, followed by 0.0044 g of $Zn(NO_3)_3{\cdot}6H_2O$ and 0.0848 g of $Fe(NO_3)_3{\cdot}9H_2O$ (Scheme 2). A black color resulted from adding 0.0184 g of CH_3COONa after the salts had been completely dissolved. A gentle dropwise addition of 9 ml ethylenediamine (EDA) was added to the mixture, and the mixture was thoroughly mixed for a few minutes. A Teflon-lined autoclave containing the whole mixture was put in a 200 °C electric oven for 24 h, and then the mixture was washed with distilled water and ethanol, followed by 24 h vacuum storage at 50 °C [27].

Scheme 2 The schematic procedures for the synthesis of Zn-doped Fe_3O_4 magnetic nanosheets

2.5 Preparation of a real sample

To deproteinize serum samples, 5 ml of trichloroacetic acid (TCA) was added and centrifuged for 5 min at 5000 rpm. Following deproteinization, human serum was diluted with pure water and considered to be a real sample.

2.6 Preparation of GO/GCE

To remove physical adsorbates and ensure a clean electrode surface, at first, different sizes of alumina slurry were used to polish the GCE and sonicate for 2 min in a mixture of water and ethanol. To prepare a fresh dispersion of graphene oxide (GO), under sonication, 5 mg of GO was utilized to make a 5 mg/ml GO solution with double-distilled water. Onto the previously cleaned GC disk electrode, 10 µl of the solution was drop-cast, and it was then dried under vacuum at room temperature.

2.7 Preparation of GO/Zn-doped Fe_3O_4Ns/GCE

In a solution of 2 ml dimethylformamide (DMF), 1 mg of GO and 1 mg of Zn-doped Fe_3O_4Ns were ultrasonically agitated to form a suspension. A 10 µl coating of GO/Zn-doped Fe_3O_4Ns was applied to the glassy carbon electrode surface, after which electrochemical testing was conducted on the modified electrode.

3 Results and discussion

3.1 Characterization of GO

It is often possible to identify graphene oxide (GO) through its UV absorption, so this technique was used to characterize it. According to Fig. S3, graphene oxide (GO) has a major absorption peak at 237 nm due to the π–π* transition of atomic C–C bonds, followed by a shoulder peak at 300 nm due to aromatic C–C bond n–π*transitions [28].

The oxide form of graphite, GO, contains more oxygen-containing functional groups due to the oxidation process. As seen in Fig. S4, a broad and intense peak was observed at a wavelength of 3398 cm^{-1}, confirming the existence of an O–H bond (hydroxyl group). Aside from that, C–O–C stretching (epoxy group) can be observed at wavelengths of 1227 and 1036 cm^{-1}, whereas –C=O stretching (–COOH group) can be observed at wavelengths of 1729 cm^{-1}. GO's edges and basal plane are intensely occupied by oxygen molecules (O) due to all these carboxylic, hydroxyl, epoxide, and carbonyl groups [29].

To investigate graphene oxide, X-ray diffraction analysis (XRD), one of the most commonly used methods for crystalline material characterization, was used. (Fig. S5). A pure graphite diffraction peak is found at around 26° due to its 0.335 nm interlayer distance [30]. It is confirmed here that graphene oxide shows a diffraction peak at 2θ around 12.1° with d-spacing = 0.77 nm. The peak at 26° has completely disappeared after treatment with graphite oxidation and exfoliation, resulting in oxygen-containing functional groups forming. In addition, XRD experiment was used to study the structure of Fe_3O_4Ns and Zn-doped Fe_3O_4Ns. According to Fig. 1a, cubic single-phase Fe_3O_4Ns are correlated with the dominant peaks at 27.23°, 45.44°, 56.20°, 66.12°, 83.88°, and 90.30°. It is evident from the sharp peaks in the XRD spectrum that the particles have excellent fineness and small crystal sizes. It was found that neither zinc as a pure metal, nor zinc oxide, nor binary phases of zinc were present in this experiment. In Fig. 1a, Zn-doped Fe_3O_4Ns are also illustrated by the XRD pattern. Adding Zn^{2+} to Fe_3O_4Ns decreases the intensity and broadens the width of diffraction peaks.

In Fig. 2(a, b, c, d), typical TEM images are also used to illustrate the morphology of Zn-doped Fe_3O_4Ns. The best nanosheet structure can be seen in large quantities at different magnifications, indicating that Zn-doped Fe_3O_4Ns have the best nanosheet structure.

A vibrating sample magnetometer (VSM) analysis was performed to investigate the magnetic properties of Fe_3O_4Ns doped with Zn^{2+} (Fig. 3). It is essential to determine a sample's magnetic properties based on its saturation magnetization (Ms) value. In this case, Ms reached 70, showing that Zn-doped Fe_3O_4Ns are highly magnetized.

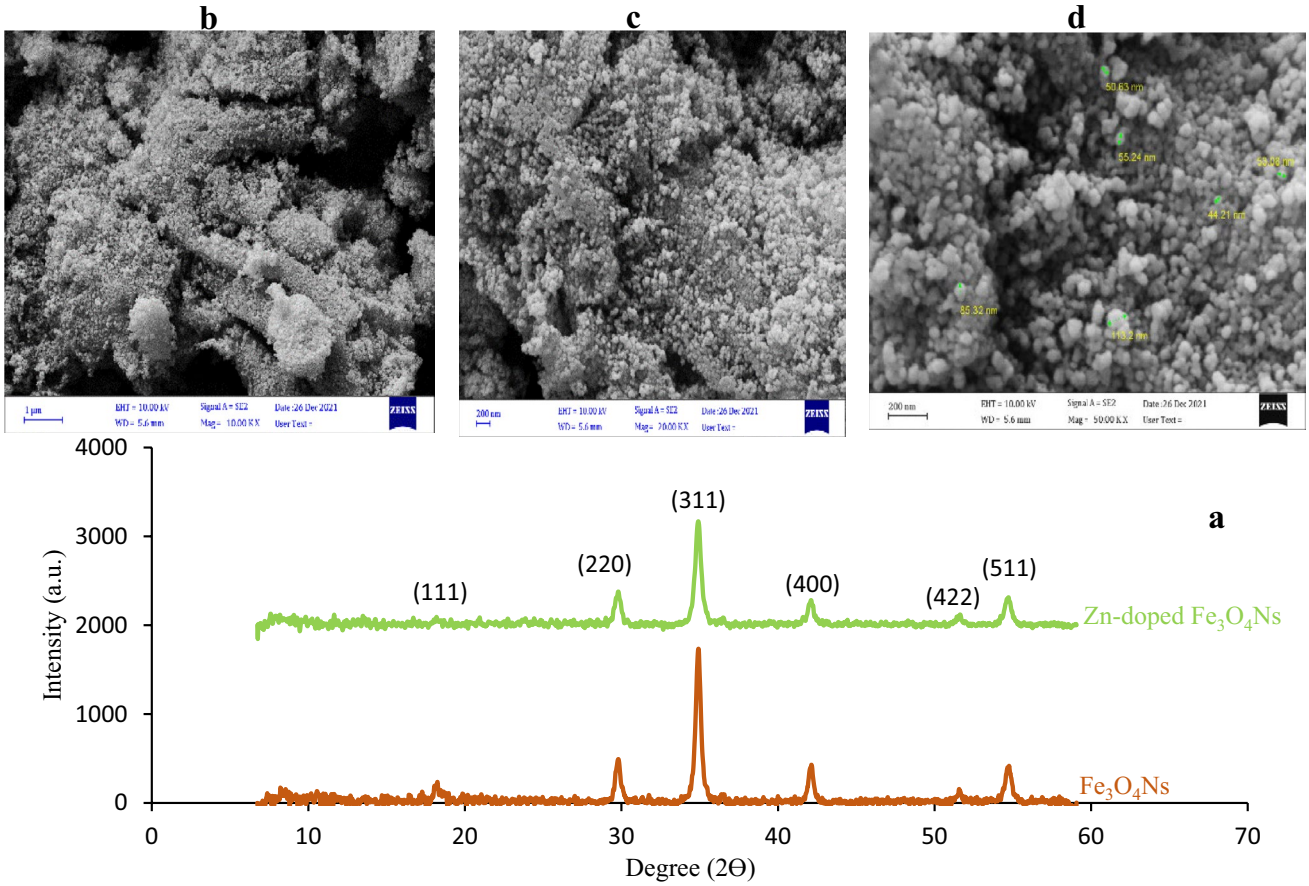

Fig. 1 The XRD patterns of **a** the pure Fe_3O_4Ns and Zn-doped Fe_3O_4Ns and **b**, **c**, **d** FESEM images of Zn-doped Fe_3O_4Ns

For the identification of their structure and functional groups, FTIR measurements were conducted on the Zn-doped Fe_3O_4Ns and Fe_3O_4Ns. Figure 4 clearly shows that surface water molecules caused the peaks at approximately 3417 and 1626 cm^{-1}, indicating the stretching and bending of O–H atoms. A broad and sharp peak at 575 cm^{-1} is caused by the vibration of the Fe–O bond. In Zn-doped Fe_3O_4Ns nanosheets, the Zn–O vibrations peak at 457 cm^{-1}, suggesting that Zn could be present in this composition. However, Fe_3O_4Ns did not exhibit such vibrations [31]. As a result of the effective doping of Zn^{2+}, Zn-doped Fe_3O_4Ns show a lower intensity of Fe–O bond vibrations in the FTIR spectrum.

The elemental composition of the sample was determined using EDS spectral analysis. Several elements, including Zn, Fe, C, N, O, and Au, can be seen in Fig. 5. The sample was coated with a thin sheet of gold to enhance conductivity and allow electric charge to flow, and this caused the peak corresponding to Au to appear in the EDS analysis. The presence of a peak corresponding to Zn indicates that the nanosheets are composed of this element. Map analysis is a new technique for displaying an atom's presence in a material. Figure 5 illustrates the good distribution of every atom, particularly Zn and Fe.

3.2 Electrochemical studies of modified GO/Zn-doped Fe_3O_4Ns/GCE

A cyclic voltammetry method was used to investigate the electrochemical properties of GO/Zn-doped Fe_3O_4Ns/GCE, GO/GCE, and GCE at different scan rates in 4 mM $[Fe(CN)_6]^{3-/4-}$containing 0.1 M phosphate buffer (PH 7.0) as a redox probe (Fig. S6a, b, c). Due to electrostatic repulsion, the intensity of peak current has decreased in the presence of modifier GO. However, when modifier GO/Zn-doped Fe_3O_4Ns are present, the peak current intensity increases. Modified and unmodified electrodes were evaluated using the Randles–Sevcik equation for reversible processes:

$$I_{pa} = (2.69 \times 10^5) A\, n^{3/2} D^{1/2} C_0\, \upsilon^{1/2}$$

According to the slopes of I_{pa} versus $\upsilon^{1/2}$ of the Randles-Sevik equation (Fig. S6d, e, f) with GO and Zn-doped Fe_3O_4Ns, the electrode surface area increased 17.15 times.

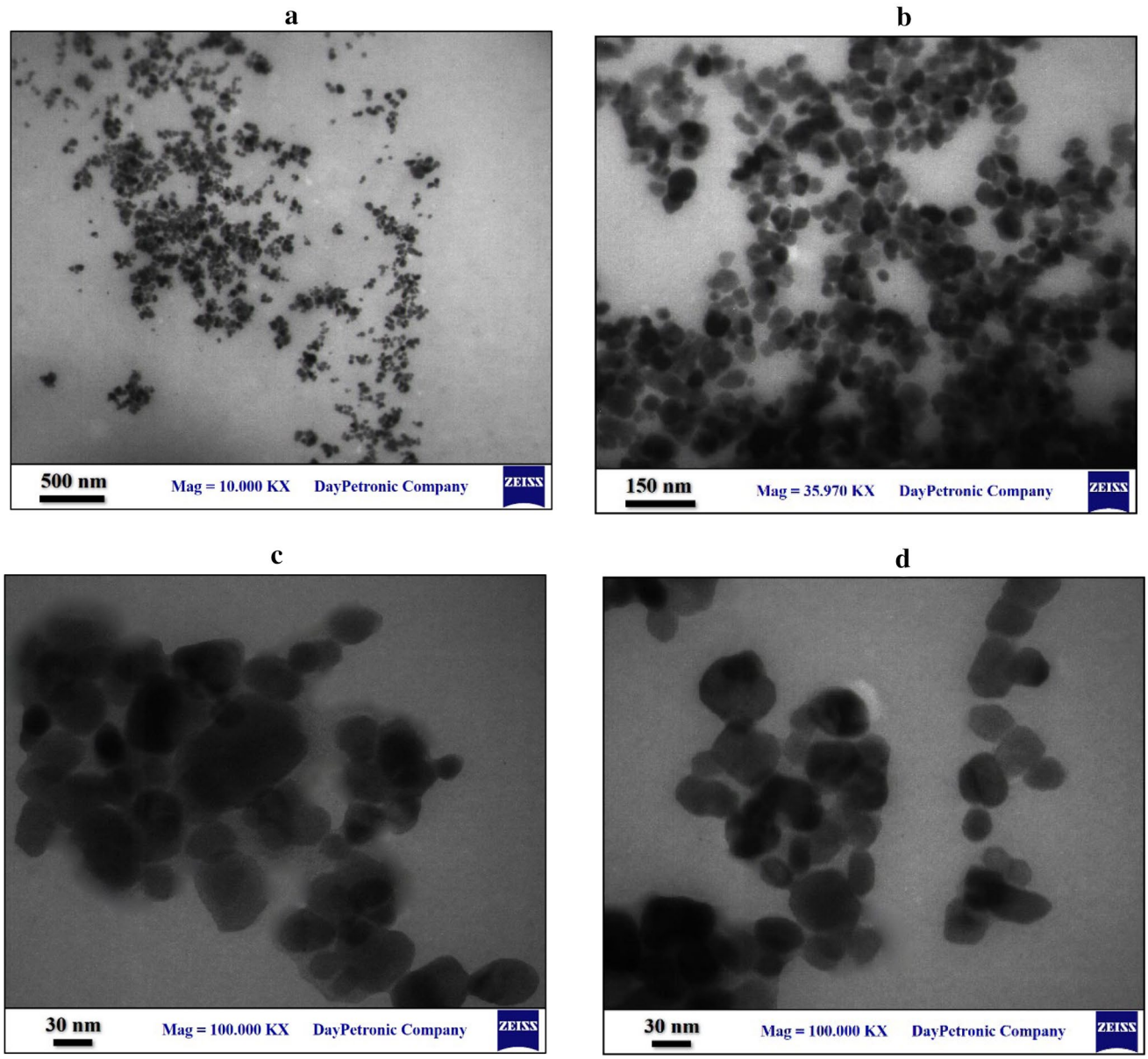

Fig. 2 TEM images of Zn-doped Fe_3O_4Ns

As a result, Zn-doped Fe_3O_4Ns are more electrocatalyst active and have a higher active surface area.

3.3 The electrochemical impedance spectroscopy (EIS) technique

The characteristics of interfacial electron-transfer between electrodes can be determined by electrochemical impedance spectroscopy (EIS). The linear part of the semicircular diameter represents diffusion in an impedance spectrum, while the semicircular diameter represents electron-transfer resistance [32, 33]. A study was conducted using electrochemical impedance spectroscopy (EIS) to examine the characteristics of electron transport between GCE with and without the modifier. As illustrated in Fig. 6, Nyquist plots of the GCE, GO/GCE, and GO/Zn-doped Fe_3O_4Ns/GCE are shown in a solution of 0.1M KCl containing 4 mM $[Fe(CN)_6]^{3-/4-}$. At high frequencies, a semicircle can be observed on the bare GCE, indicating an increased resistance of the electrode surface. Based on the Nyquist plots, we can observe that GO has a greater semicircle than GC, which suggests that the semiconducting property of GO causes issues with interfacial charge transfer. A significant reduction in charge transfer resistance was achieved by adding Fe_3O_4Ns to GO. The GCE modified with GO and Zn-doped Fe_3O_4Ns exhibited the least electrode surface resistance, which confirms that by modifying the sensor with GO and Zn-doped

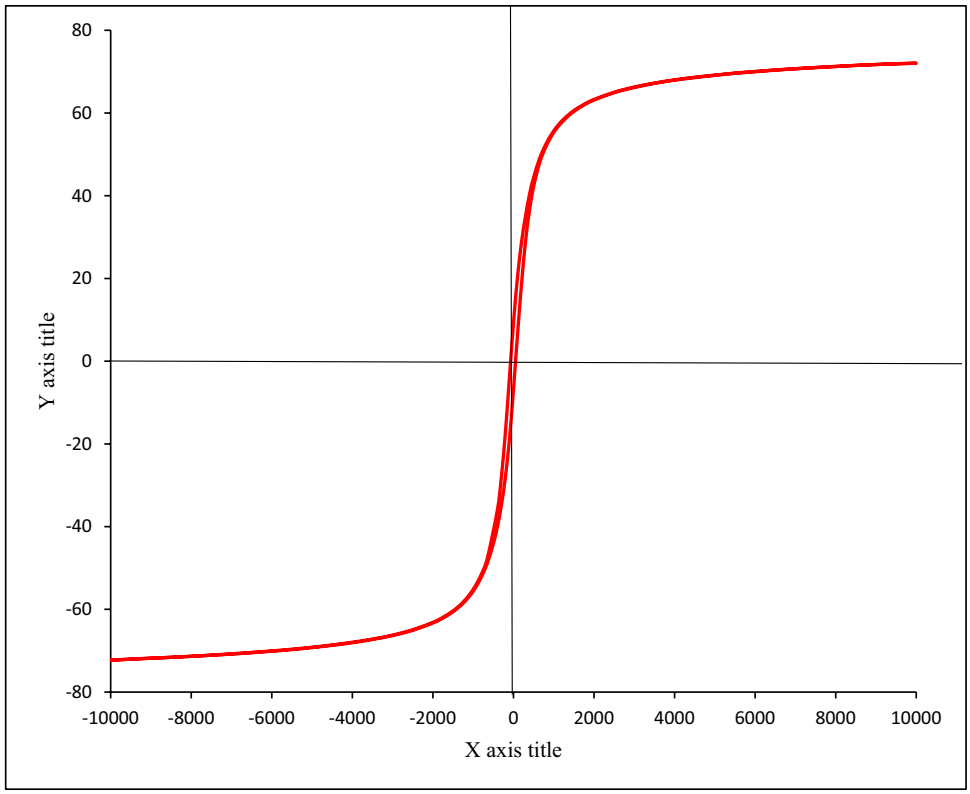

Fig. 3 VSM analysis of Zn-doped Fe_3O_4Ns

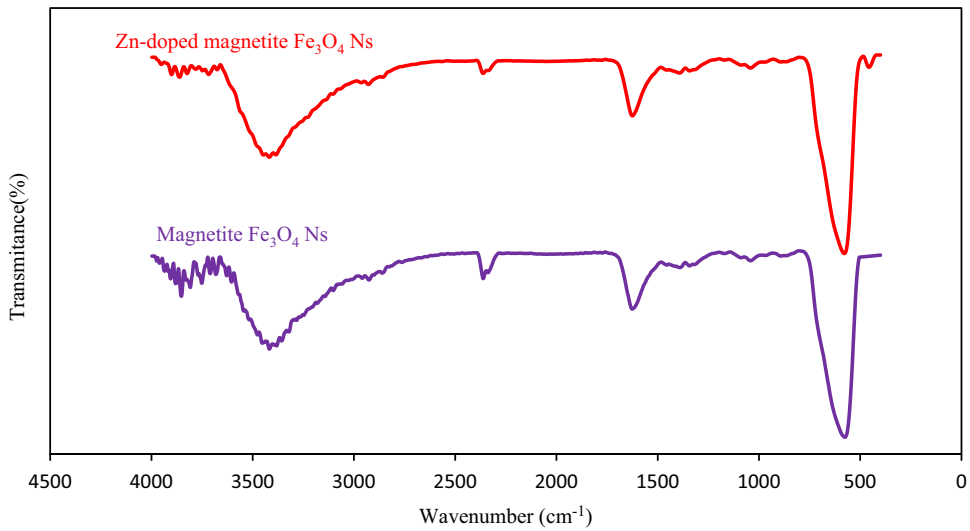

Fig. 4 FTIR analysis of the pure Fe_3O_4Ns and Zn-doped Fe_3O_4Ns

Fe_3O_4Ns, its conductivity can be improved, allowing it to be used as a dual-purpose electroanalytical sensor for measuring both GA and AD.

3.4 Influence of supporting electrolyte and pH of supporting electrolyte

A differential pulse voltammetry experiment was conducted on GO/Zn-doped Fe_3O_4Ns/GCE electrochemical

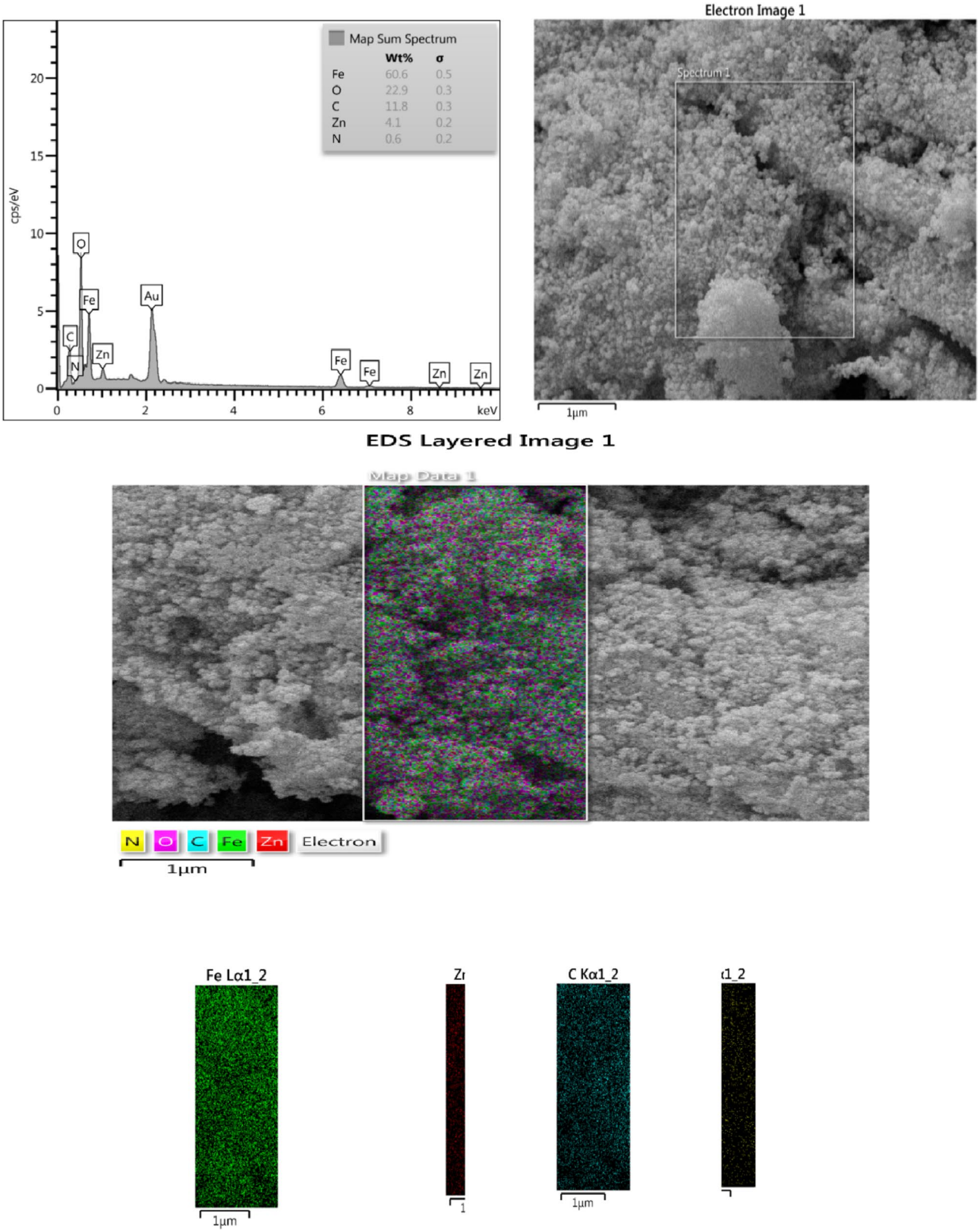

Fig. 5 The EDS spectral analysis and map analysis of Zn-doped Fe_3O_4Ns

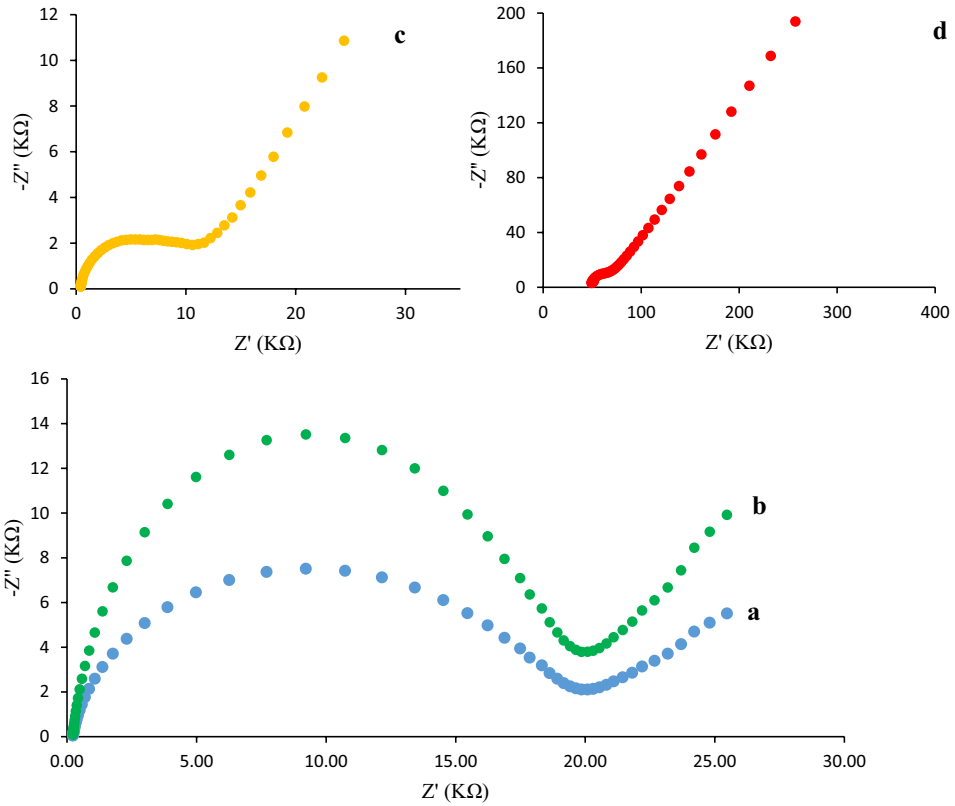

Fig. 6 Nyquist plots of **a** GCE, **b** GO/GCE, **c** GO/Fe_3O_4Ns/GCE, and **d** GO/Zn-doped Fe_3O_4Ns/GCE in solutions of 0.1 M KCl containing 4 mM $[Fe(CN)_6]^{3-/4-}$

performance using 0.1 M acetate buffer solution (ABS), Britton–Robinson buffer solution (BRS), citrate buffer solution (CBS), and phosphate buffer solution (PBS). (Fig. S7). For the remaining electrochemical test, 0.1 M BRS was selected as the ideal supporting electrolyte because GO/Zn-doped Fe_3O_4Ns/GCE presented the best electrochemical response to both GA and AD.

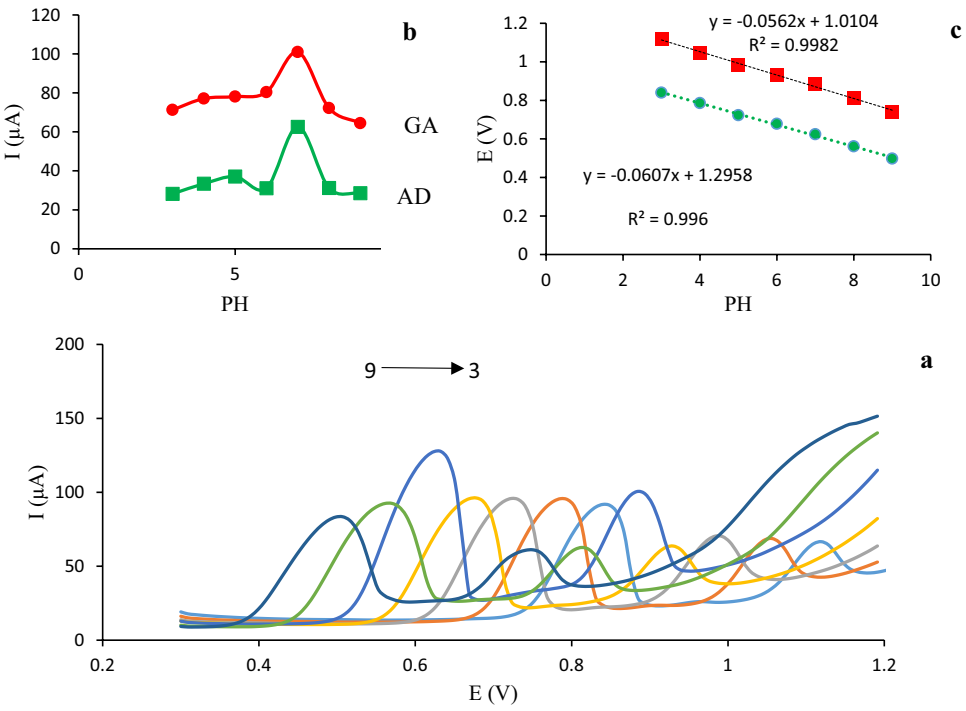

Fig. 7 **a** Differential pulse voltammetry of GA and AD at the surface of the GO/Zn-doped Fe_3O_4Ns/GCE at various pHs **b** the relationship of the oxidation peak current and **c** oxidation peak potential with pH

A DPV measurement has been performed for GA and AD solutions containing 0.1 M BRS to investigate the impact of pH on the electrochemical response of modified electrodes (Fig. 7a). Figure 7b shows that the anodic peak currents (I_{pa}) increase from pH 3.0 to 7.0, then decrease dramatically; thus, pH 7.0 has been determined to be the optimum pH for further electrochemical tests. As a result of applying the dEp/dpH equation, whose slope is − 2.303 mRT/nF, where m and n represent protons and electrons, 0.0562 and 0.0607 slopes were obtained for GA and AD, respectively (Fig. 7c). As the slope of the Nernstian value is 0.059 V/pH, along with the values of the slopes, we can assume the electrochemical process of GA and AD involves an equal number of electrons and protons.

3.5 The accumulation time effect

For GA and AD, accumulation time affected the electrochemical response. Fig. S8 shows that GA and AD oxidation peak currents increase from 0 to 40 s, and then the oxidation peak current decreases due to a limited electron-transfer between the electrode and GA and AD. It was therefore decided that the 40s were the best time for accumulation.

3.6 GA and AD electrochemical behavior on different electrode surfaces

An experiment was conducted to investigate the effect of GO and Zn-doped Fe_3O_4Ns on the electrode surface using differential pulse voltammetry (DPV) in 5 µM GA and 5 µM AD containing BRS at pH 7.0. Figure 8 shows differential pulse voltammetry measurements on GCE, GO/GCE, and GO/Zn-doped Fe_3O_4Ns/GCE. As can be seen, bare GCE does not exhibit sensitivity to GA and AD, while modification with GO increases these currents. A significant increase in the oxidation peak current of GA and AD occurs when Fe_3O_4Ns are added to GO. The highest currents.

were observed at GCE modified with GO and Zn-doped Fe_3O_4Ns. A large surface area and high electrical conductivity of the GO/Zn-doped Fe_3O_4Ns nanocomposite contributed to these results. GA and AD oxidation peaks at low positive potentials indicate high electro-catalytic activity of Fe_3O_4Ns doped with Zn^{2+}, so GO/Zn-doped Fe_3O_4Ns / GCE was used for simultaneous GA and AD electrochemical measurements.

3.7 Influence of scanning rate

A CV experiment was conducted at GO/Zn-doped Fe_3O_4Ns/GCE to explore the effect of scan rate on peak currents (Ipa) for GA and AD in BRS solution at pH 7.0 (Fig. 9). Using CV, investigators can uncover the electrochemical mechanism through an analysis of the peak current-scanning rate relationship. In Fig. 9 (insets), the anodic peak currents of GA and AD have linear relationships with scanning rate (υ) within ranges between 10 and 100 mV/s. This observation is correlated with the linear regression equation:

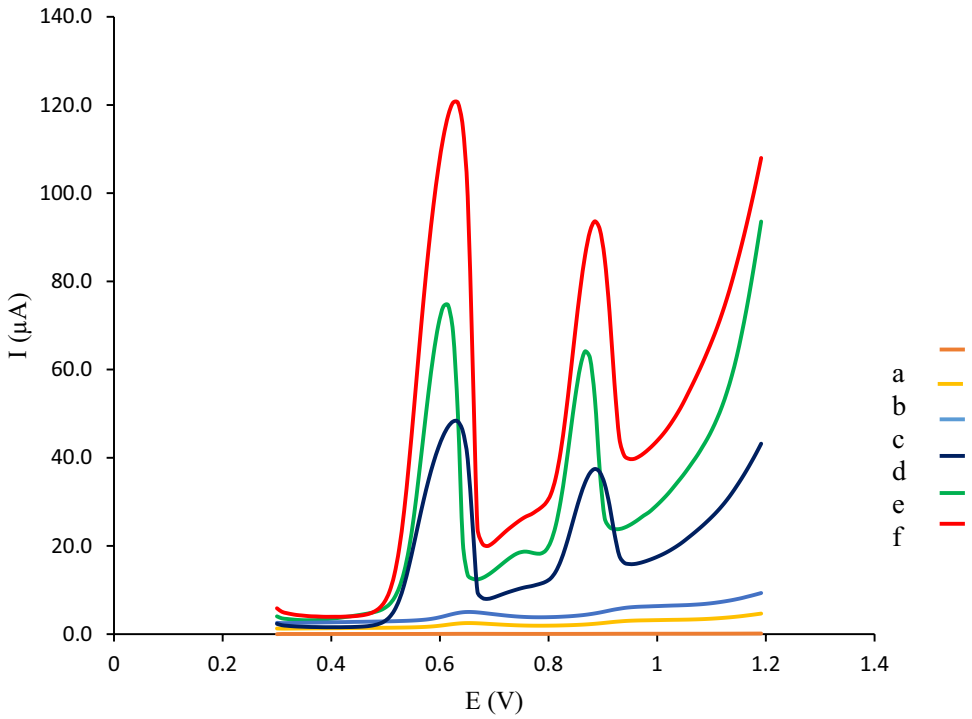

Fig. 8 Differential pulse voltammetry of **a** unmodified GCE and **c** GO/Zn-doped Fe_3O_4Ns/GCE in 0.1 M BRS (pH 7.0), **b** unmodified GCE, **d** GO/GCE, **e** GO/Fe_3O_4Ns/GCE, and **f** GO/Zn-doped Fe_3O_4Ns/GCE in 5.0 µM GA and 5.0 µM AD containing 0.1 M BRS

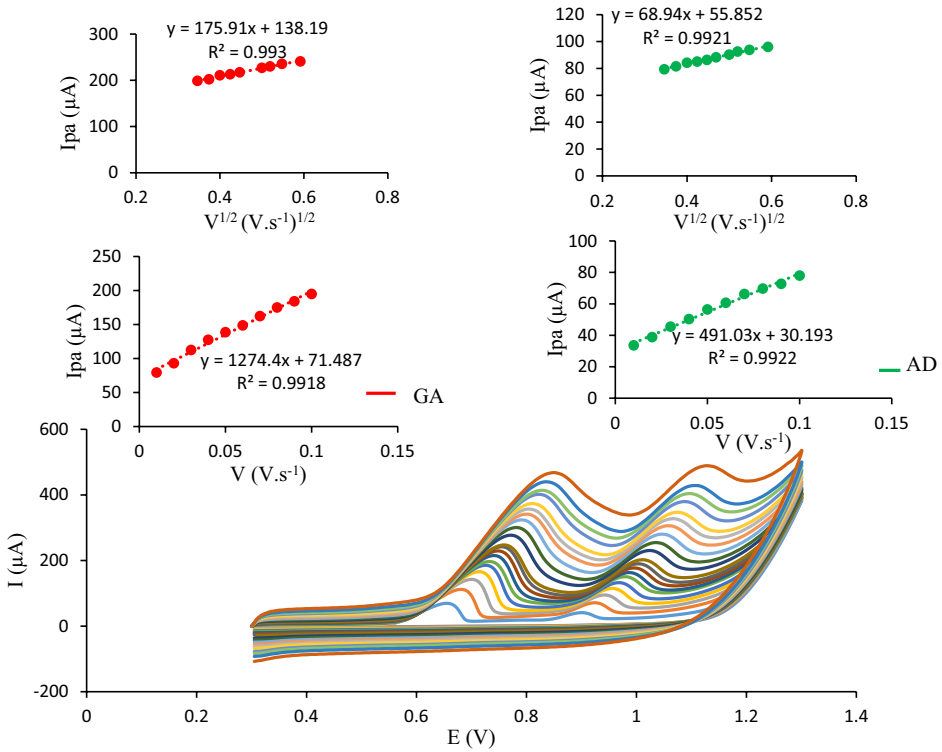

Fig. 9 Cyclic voltammograms of 5.0 µM GA and 5.0 µM AD at the surface of GO/Zn-doped Fe_3O_4Ns/GCE in 0.1M BRS (pH 7.0) at different scan rates from 10 to 350 mV/s, inset: plot of I_{pa} vs. υ and I_{pa} vs. $\upsilon^{1/2}$ for GA and AD

$$\text{GA}: I_{pa}(\mu\text{A}) = 1274.4\,\upsilon\,(\text{V s}^{-1}) + 71.487 \quad R^2 = 0.991,$$

$$\text{AD}: I_{pa}(\mu\text{A}) = 491.03\,\upsilon\,(\text{V s}^{-1}) + 30.193 \quad R^2 = 0.992.$$

At sweep rates above 100 mV/s for GA and AD, the relationship between peak current and the square root of the scan rate ($\upsilon^{1/2}$) linearized. The following are the linear regression equations:

$$\text{GA}: I_{pa}(\mu\text{A}) = 175.91\,\upsilon^{1/2}(\text{V s}^{-1})^{1/2} + 138.19 \quad R^2 = 0.993,$$

$$\text{AD}: I_{pa}(\mu\text{A}) = 68.94\,\upsilon^{1/2}(\text{V s}^{-1})^{1/2} + 55.85 \quad R^2 = 0.992.$$

These results suggest that the electron-transfer reactions of GA and AD at GO/Zn-doped Fe_3O_4Ns/GCE surfaces are controlled both by adsorption and diffusion.

A charge transfer coefficient (α) and electron-transfer rate constant (ks) for an irreversible anodic reaction can be calculated using Laviron's theory based on the difference between Ep and Ln υ [34].

$$E_p = E_0 - \left(\text{RT}/\alpha_a\text{nF}\right)\ln\left(\text{RTKs}/\alpha_a\text{nF}\right) + \left(\text{RT}/\alpha_a\text{nF}\right)\ln\upsilon.$$

To calculate the formal potential (E_0), we can extrapolate the E_P versus υ curve to the vertical axis at $\upsilon = 0$ [35]. With E_p versus lnυ and the slope of the straight line, α_a for GA and AD were calculated to be 0.26 and 0.21, whereas Ks for GA and AD were calculated with E_0 and α_a, resulting in 0.59 and 0.45 s^{-1}, respectively (Fig. S9). Consequently, the GO/Zn-doped Fe_3O_4Ns nanocomposite exhibits a demonstrable ability to enhance electron-transfer between analytes and electrodes.

3.8 Chronoamperometric measurement of GA and AD

Chronoamperometry is an electrochemical method for determining species diffusion coefficients on electrode surfaces, so CA measurements were conducted for GO/Zn-doped Fe_3O_4Ns/GCE to obtain the GA and AD diffusion coefficients (D) (Fig. 10a, c)

According to the Cottrell equation:

$$I = n\,F\,D^{1/2}A\,C_0\pi^{-1/2}t^{-1/2}.$$

In diffusion control conditions, D can be found by plotting I versus $t^{-1/2}$ with a slope equal to the value of D, so in Fig. 10b, d, we plot I versus $t^{-1/2}$ for GA and AD. According to this study, the diffusion coefficients (D) for GA and DA are 16.0×10^{-5} cm^2/s and 15.9×10^{-5} cm^2/s, respectively. Therefore, GA and AD are very well diffused at the modified electrode's surface.

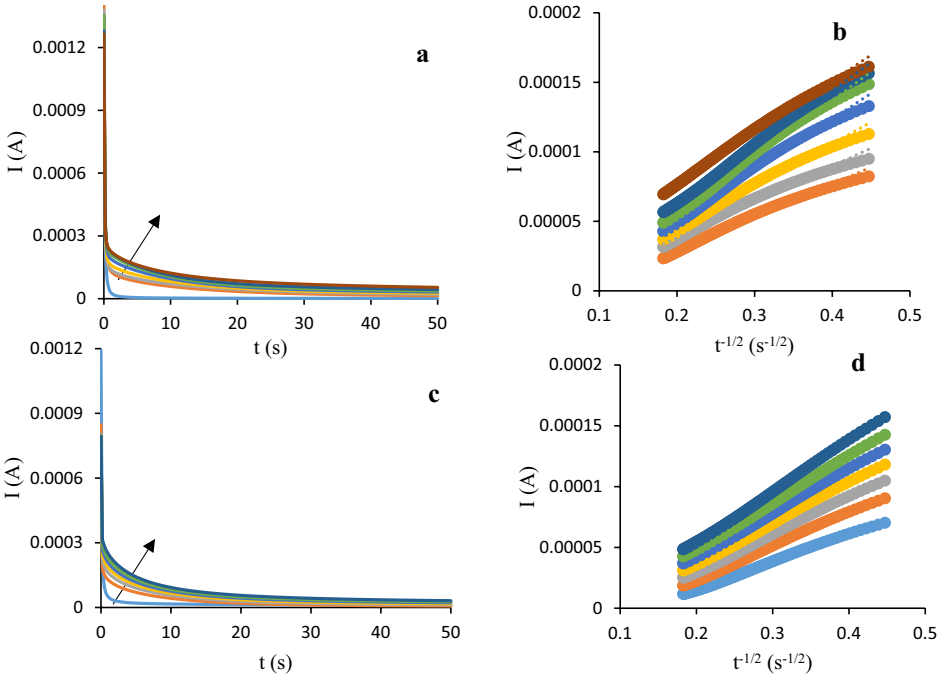

Fig. 10 Chronoamperogram measurements of GO/Zn-doped Fe_3O_4Ns/GCE in 0.1 M BRS (pH 7.0) **a** in the presence of 50 µM, 100 µM, 150 µM, 200 µM, 250 µM, 300 µM, 350 µM of GA and **c** in the presence of 50 µM, 100 µM, 150 µM, 200 µM, 250 µM, 300 µM, 350 µM of AD. Plots of I vs. $t^{-1/2}$obtained from chronoamperograms for **b** GA and **d** AD

3.9 Limits of detection and calibration curve

Differential pulse voltammetry was used to determine GA and AD simultaneously in the range of 0.05–10 µM and 10–500 µM, respectively (Fig. 11). GA anodic peak currents were proportional to concentration for two concentration ranges 0.05–10 µM and 10–500 µM, represented by linear regression equations I_{pa} (µA) = 10.2 C (µM) + 45.1 and I_{pa} (µA) = 0.510 C (µM) + 145.96, respectively (Fig. 11a, b, c). A linear relationship between anodic peak current and AD concentration is shown in the graphs between 0.05–10 µM and 10–500 µM, via linear regression equations: I_{pa} (µA) = 5.84 C (µM) + 35.82 and I_{pa} (µA) = 0.332 C (µM) + 95.26 (Fig. 11d, e, f). The LOD is defined as the limit of detection (LOD) determined by the equation $LOD = KS^0/S$, where K is a constant associated with the confidence level, S^0 is the standard deviation of ten blank-solution measurements (without GA and AD), and S is the calibration curve slope. A low detection limit (LOD) of 0.08 µM was calculated for GA and 0.14 µM for AD, indicating that the suggested electrode has a large linear dynamic range, good sensitivity, and a low detection limit.

3.10 GO/Zn-doped Fe_3O_4Ns/GCE repeatability and stability

The suggested sensor's repeatability was evaluated using ten repeated tests of 10 µM GA and 10 µM AD solutions. In each measurement, the modified electrode was washed with a 2 N NaOH solution to remove the GA and AD molecules. Therefore, GA and AD each showed a relative standard deviation of 2.65% and 3.91%, respectively.

The proposed sensor was also tested for stability after being kept in 0.1 M BRS (pH 7.0) or air for a defined time. Under wet conditions, the DPV measurements of GA and AD were made after the sensor was immersed in 0.1 M BRS (pH 7.0). The response current of this sensor decreased by 4.32% and 4.64%, respectively, after being tested six times for 12.5 h. According to these results, the modified electrode was very stable under dry conditions, since both GA and AD sensors maintained 94.74 and 91.71% of their initial electrochemical responses over 7 days, respectively.

3.11 Effect of interference on the electrochemical response

To investigate the selectivity of the proposed sensor for determining GA and AD, different interfering species were added to a mixture of GA and AD solutions. A tolerance limit indicates which concentration of interfering species will result in less than 10% error in the analyte peak current, as shown in Table 1. Throughout the table, interfering species are not found to affect quantitative measurements of guanine and adenine.

3.12 Real sample analysis

As a means of preventing matrix effects, the standard addition method for GA and AD was used to test the modified electrode in serum samples. The relative standard deviation

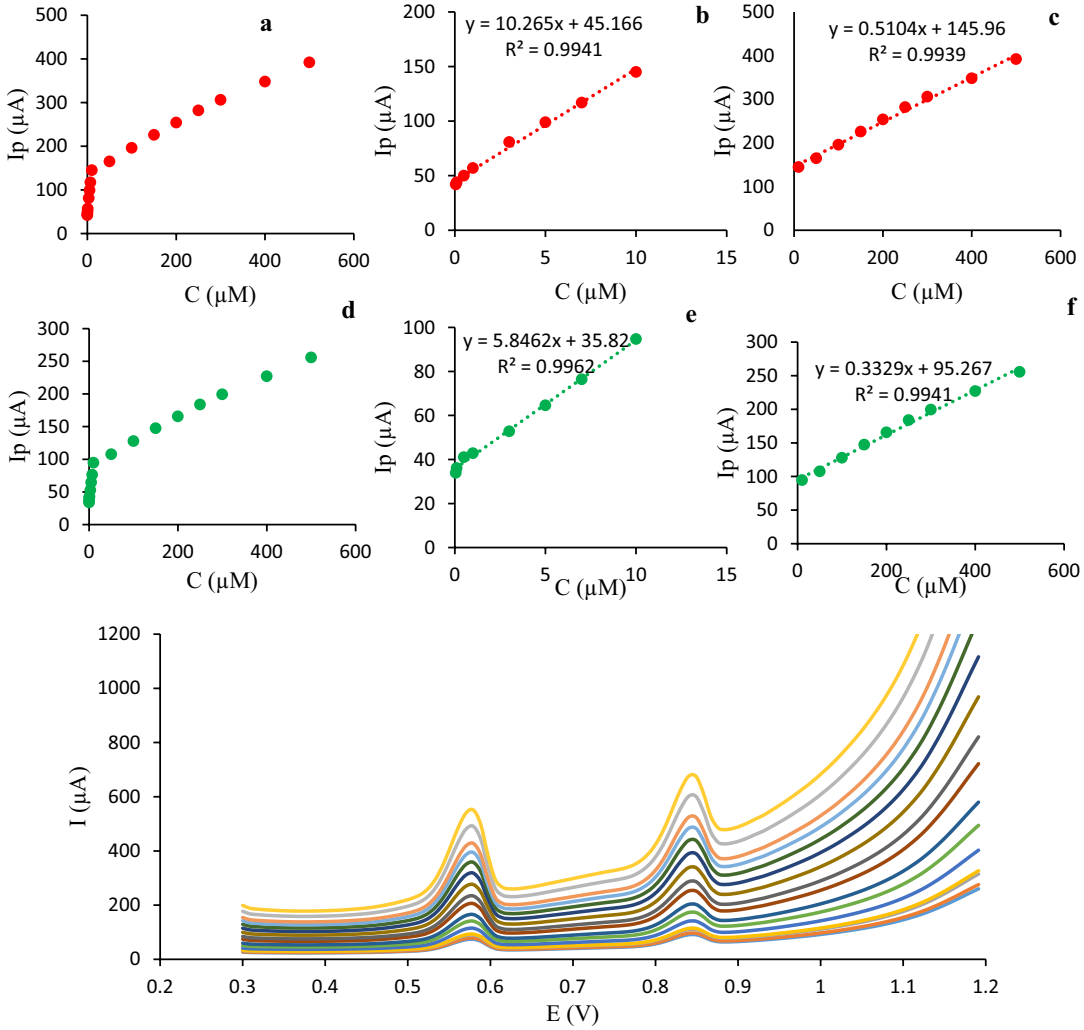

Fig. 11 Differential pulse voltammograms of GO/Zn-doped Fe_3O_4Ns/GCE in different concentrations of GA and AD in 0.1 M BRS. Insets: The plot of I_{pa} vs. C from **a** 0.05–500 μM, **b** 0.05–10 μM, and **c** 10–500 μM for GA, and the plot of I_{pa} vs. C from **d** 0.05–500 μM, **e** 0.05–10 μM, and **f** 10–500 μM for AD

Table 1 An investigation of interference in the determination of guanine and adenine

Interference	GA C_{int} (μM)	AD C_{int}(μM)
Ascorbic acid	900	600
Uric acid	400	900
Acetaminophen	550	800
Tryptophan	950	550
Dopamine	600	850
Glucose	1200	500
Epinephrine	650	1000
Hydrochlorothiazide	800	450

and recovery data are shown in Table 2. The electrochemical sensor proved capable of detecting GA and AD in real sample solutions, regardless of the matrix, with recovery rates ranging from 96.3 to 101.78%, and RSDs of 1.2–1.5%.

4 Conclusion

An electrochemical sensor, which is both innovative and highly sensitive, was developed for the simultaneous measurement of GA and AD. The Zn-Fe_3O_4Ns/GO/GCE exhibited significantly improved responses for GA and AD, attributed to the increased surface area and high electro-catalytic activity of Zn-Fe_3O_4Ns. Additionally, the incorporation of GO with Zn-Fe_3O_4Ns enhanced the sensor's sensitivity to the oxidation of GA and AD compounds in solutions. The

Table 2 An analysis of the levels of guanine and adenine in a human serum sample

Spiked (μM)		Found*		R.S.D. (%)		Recovery (%)	
GA	AD	GA	AD	GA	AD	GA	AD
0	0	˂ DL	˂ DL	–	–	–	–
3	3	2.94	2.88	1.4	1.5	98.00	96.30
100	100	98.11	101.78	1.2	1.3	98.11	101.78

∗Average of three measurements at optimum conditions

results indicated that the proposed sensor possesses excellent characteristics such as easy preparation, exceptional stability and sensitivity, a wide linear dynamic range, low detection limits, excellent repeatability, and high tolerance to common interference agents. Moreover, the modified electrode demonstrated good recovery for determining analytes in real samples, thus highlighting the potential applicability of Zn-Fe_3O_4Ns/GO/GCE as an ideal candidate for electrochemical sensor applications.

Supplementary Information The online version contains supplementary material available at https://doi.org/10.1007/s10800-024-02072-5.

Author contributions All authors contributed to the study conception and design. RN was involved in material preparation, analysis and data collection. He also wrote initial draft of the manuscript and all authors commented on the previous version of the manuscript. AB advised in methodology of experiments and supervised the study. All authors read the final version of the manuscript and approved it.

Funding The authors gratefully acknowledge the research council of Arak University for providing financial support for this work.

Data availability The data that support the findings of this study are available from the corresponding author upon reasonable request.

Declarations

Conflict of interest The authors declare no conflicts of interest.

Ethical approval Not applicable.

References

1. Feng L, Chen Y, Ren J, Qu X (2011) A graphene functionalized electrochemical aptasensor for selective label-free detection of cancer cells. Biomaterials 32:2930–2937
2. Villalonga A, Estabiel I, Pérez-Calabuig AM et al (2021) Amperometric aptasensor with sandwich-type architecture for troponin I based on carboxyethylsilanetriol-modified graphene oxide coated electrodes. Biosens Bioelectron 183:113203
3. Garcia SM, Wong A, Khan S, Sotomayor MDPT (2021) A simple, sensitive and efficient electrochemical platform based on carbon paste electrode modified with Fe_3O_4@ MIP and graphene oxide for folic acid determination in different matrices. Talanta 229:122258
4. Shahriari S, Sastry M, Panjikar S, Raman RKS (2021) Graphene and graphene oxide as a support for biomolecules in the development of biosensors. Nanotechnol Sci Appl 14:197
5. Lakshmanan P (2019) Graphene–carbon nitride-based electrochemical sensors for biomolecules. In: Pandikumar A, Rameshkumar P (eds) Graphene-based electrochemical sensors for biomolecules. Elsevier, Amsterdam, pp 207–233
6. Singh M, Bhardiya SR, Patel D et al (2024) Electrocatalytic quantification of quinol in cosmetic samples using co-doped graphitic carbon nitride@ biomolecule assisted electrochemically reduced graphene nanosheets. Talanta 269:125400
7. Krishnan SK, Singh E, Singh P et al (2019) A review on graphene-based nanocomposites for electrochemical and fluorescent biosensors. RSC Adv 9:8778–8881
8. Shanbhag YM, Shanbhag MM, Malode SJ et al (2022) 2D graphene sheets as a sensing material for the electroanalysis of zileuton. Catalysts 12:867
9. Cheng Z, Song H, Li Z et al (2023) Hierarchical composites based on near-spherical ZnO attached on nitrogen-doped reduced graphene oxide for enhanced nitrite electrochemical sensing property. Microchem J 197:109764
10. Salih E, Mekawy M, Hassan RYA, El-Sherbiny IM (2016) Synthesis, characterization and electrochemical-sensor applications of zinc oxide/graphene oxide nanocomposite. J Nanostructure Chem 6:137–144
11. Sebastian N, Yu W-C, Balram D (2019) Electrochemical detection of an antibiotic drug chloramphenicol based on a graphene oxide/hierarchical zinc oxide nanocomposite. Inorg Chem Front 6:82–93
12. Zhan W, Guo Y, Wang Y et al (2009) Study of higher selectivity to styrene oxide in the epoxidation of styrene with hydrogen peroxide over La-doped MCM-48 catalyst. J Phys Chem C 113:7181–7185
13. Xu J, Yang H, Fu W et al (2007) Preparation and magnetic properties of magnetite nanoparticles by sol–gel method. J Magn Magn Mater 309:307–311
14. Basak S, Chen D-R, Biswas P (2007) Electrospray of ionic precursor solutions to synthesize iron oxide nanoparticles: modified scaling law. Chem Eng Sci 62:1263–1268
15. Zhou ZH, Wang J, Liu X, Chan HSO (2001) Synthesis of Fe_3O_4 nanoparticles from emulsions. J Mater Chem 11:1704–1709
16. Salazar-Alvarez G, Muhammed M, Zagorodni AA (2006) Novel flow injection synthesis of iron oxide nanoparticles with narrow size distribution. Chem Eng Sci 61:4625–4633
17. Nehru R, Dong C-D, Chen C-W (2021) Cobalt-doped Fe_3O_4 nanospheres deposited on graphene oxide as electrode materials for electrochemical sensing of the antibiotic drug. ACS Appl Nano Mater 4:6768–6777
18. Xu J, Sun Y, Zhang J (2020) Solvothermal synthesis of Fe_3O_4 nanospheres for high-performance electrochemical non-enzymatic glucose sensor. Sci Rep 10:16026
19. Pushpagiri T, Kumar ER, Ramalingam A et al (2023) Effect of doping concentration on structural, vibrational, morphological and colloidal stability of Zn doped NiO nanoparticles for gas

sensor applications. Ceram Int. https://doi.org/10.1016/j.ceramint.2023.04.240
20. Gill BD, Indyk HE (2007) Development and application of a liquid chromatographic method for analysis of nucleotides and nucleosides in milk and infant formulas. Int Dairy J 17:596–605
21. Yeh C-F, Jiang S-J (2002) Determination of monophosphate nucleotides by capillary electrophoresis inductively coupled plasma mass spectrometry. Analyst 127:1324–1327
22. Heisler I, Keller J, Tauber R et al (2002) A colorimetric assay for the quantitation of free adenine applied to determine the enzymatic activity of ribosome-inactivating proteins. Anal Biochem 302:114–122
23. Erbao L, Bingchun X (2006) Flow injection determination of adenine at trace level based on luminol–$K_2Cr_2O_7$ chemiluminescence in a micellar medium. J Pharm Biomed Anal 41:649–653
24. Mervartová K, Polášek M, Calatayud JM (2007) Recent applications of flow-injection and sequential-injection analysis techniques to chemiluminescence determination of pharmaceuticals. J Pharm Biomed Anal 45:367–381
25. Huang Y-F, Chang H-T (2007) Analysis of adenosine triphosphate and glutathione through gold nanoparticles assisted laser desorption/ionization mass spectrometry. Anal Chem 79:4852–4859
26. Hummers WS Jr, Offeman RE (1958) Preparation of graphitic oxide. J Am Chem Soc 80:1339
27. Zhu J, Nan Z (2017) Zn-doped Fe_3O_4 nanosheet formation induced by EDA with high magnetization and an investigation of the formation mechanism. J Phys Chem C 121:9612–9620
28. Xu S, Yong L, Wu P (2013) One-pot, green, rapid synthesis of flowerlike gold nanoparticles/reduced graphene oxide composite with regenerated silk fibroin as efficient oxygen reduction electrocatalysts. ACS Appl Mater Interfaces 5:654–662
29. Low FW, Lai CW, Abd Hamid SB (2015) Easy preparation of ultrathin reduced graphene oxide sheets at a high stirring speed. Ceram Int 41:5798–5806
30. Handayani M, Sulistiyono E, Rokhmanto F et al (2019) Fabrication of graphene oxide/calcium carbonate/chitosan nanocomposite film with enhanced mechanical properties. In: IOP Conference Series: Materials Science and Engineering. IOP Publishing, p 12073
31. Zhao H, Liu R, Zhang Q, Wang Q (2016) Effect of surfactant amount on the morphology and magnetic properties of monodisperse $ZnFe_2O_4$ nanoparticles. Mater Res Bull 75:172–177
32. Bai X, Dexter SC, Luther GW III (2006) Application of EIS with Au–Hg microelectrode in determining electron transfer mechanisms. Electrochim Acta 51:1524–1533
33. Li Y, Song H, Zhang L et al (2016) Supportless electrochemical sensor based on molecularly imprinted polymer modified nanoporous microrod for determination of dopamine at trace level. Biosens Bioelectron 78:308–314
34. Laviron EJJ (1979) General expression of the linear potential sweep voltammogram in the case of diffusionless electrochemical systems. J Electroanal Chem Interfacial Electrochem 101:19–28
35. Wu Y, Ji X, Hu S (2004) Studies on electrochemical oxidation of azithromycin and its interaction with bovine serum albumin. Bioelectrochemistry 64:91–97

Authors and Affiliations

Rahem Nouraei[1] · Ali Babaei[1,2]

✉ Ali Babaei
ali.babaei08@gmail.com

[1] Department of Chemistry, Faculty of Science, Arak University, Arak, Iran

[2] Institute of Nanosciences & Nanotechnology, Arak University, Arak, Iran